Broadband mode converters in three-waveguide couplers based on quantumlike adiabatic transfer

Rim Alrifai [●],[1] Virginie Coda [●],[1,*] Toni Alhaddad,[1] Hussein Taleb,[1] Andon A. Rangelov,[2] and Germano Montemezzani [●][1]

[1]*Université de Lorraine, CentraleSupélec, LMOPS, F-57000 Metz, France*
[2]*Department of Physics, Sofia University, James Bourchier 5 Boulevard, BG-1164 Sofia, Bulgaria*

We propose a method for robust mode conversion between the two outer waveguides in a three-waveguide coupler based on analogies with quantum population transfer. Depending on the presence or absence of detuning between the propagation constants of the intermediate waveguide, the mode conversion can be analogous to the adiabatic-elimination or stimulated Raman adiabatic passage techniques. Both configurations give broadband and robust mode converters.

I. INTRODUCTION

Integrated optical devices are important elements to enhance the capacities of all-optical networks. In this context, spatial mode converters are required for mode-division-multiplexing technology, where different signals are coded on different guided modes via a single wavelength and are compatible with wavelength-division multiplexing [1]. Mode converters have received a lot of attention, and devices have been demonstrated using numerous methods. Some are based on phase matching, using adiabatic tapered couplers [2,3] or various types of grating couplers [4–8]. Some use beam shaping based, for instance, on Mach-Zehnder interferometers [9], Y junctions [10,11], asymmetric conversion [12–15], or supersymmetric conversion [16,17]. Some explicitly exploit constructive interferences such as multimode interference couplers [18–22], microring resonators [23,24], photonic crystals [25,26], and dielectric metasurfaces [27–30]. Engineered subwavelength structures are therefore frequently required, which may be difficult to fabricate and/or highly intolerant of imperfection. In the context of wavelength-division multiplexing, broadband mode converters are required and have been demonstrated with a wavelength bandwidth of tens of nanometers [7,14,18,19,27,29–31] or even of more than 100 nm in some devices [5,10,12,15,16,28,32,33].

One very promising and rich approach to get robust and broadband integrated components is to exploit similarities between quantum mechanics and wave optics [34], such as analogies with quantum adiabatic transfers. One example of particular interest is based on stimulated Raman adiabatic passage (STIRAP). In quantum physics, this technique implies a robust transfer of population between two energy levels coupled by one or more intermediate levels using multiple delayed laser pulses [35]. The remarkable feature of such systems is their high tolerance to system-parameter variations. In integrated optics, such systems can be mimicked by a coupled waveguide structure with spatially varying coupling coefficients leading to adiabatic power exchange between two external waveguides through one or more intermediate waveguides [36–38]. This has been experimentally demonstrated with success [39–41].

Mode converters or filters have been proposed based on analogies with STIRAP [4,31,42] and also with adiabatic passage via level crossing [5], with super structures [16,17,43], and with the shortcut to adiabaticity [44]. Most earlier mode converters, based on analogies with quantum adiabatic transfer, use a single waveguide where the input mode evolves to the desired mode along the guided propagation. The conversion is achieved thanks to coupling between the different modes of the multimode waveguide designed using computer-generated planar holograms, which correspond to complex multiplexed gratings. In the present paper, our goal is to exploit further analogies with robust adiabatic transfers, with no complex longitudinal modulation of waveguides, such as gratings; with no modulation at all of the propagation constants; and with no subwavelength designs, which are always difficult to implement.

One particularly interesting and very recent alternative is to consider a system designed with three or more evanescently coupled waveguides [32,43,45] to conceive broadband devices. In the present work, one mode enters the input waveguide (WGI) and is converted to another mode in the output waveguide (WGO) through an intermediate one (WG2). For an efficient coupling, the propagation constant of WGO of the desired output mode is phase matched with the propagation constant of the injected mode in WGI. In a STIRAP-like configuration, WG2 is also phase matched. However, in this paper, we show that this condition is not mandatory to achieve mode conversion. When a strong mismatch occurs, the transfer becomes analogous to adiabatic elimination (AE) in quantum physics [46–50]. This second technique also has the advantage of relaxing the constraint of the counterintuitive (CI) order of the coupling constants required for STIRAP. Section II describes the theory underlying mode conversion in a three-coupled-waveguide system under the STIRAP or AE configuration in the framework of the coupled-mode theory. Section III numerically verifies the expectations by means of
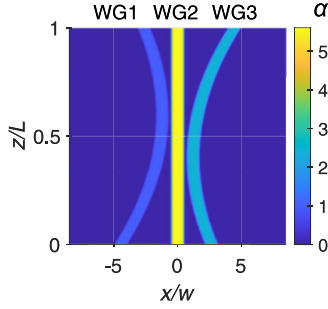
─────────
*coda5@univ-lorraine.fr

FIG. 1. Example of a structure of three coupled adiabatic waveguides used for mode conversion. The color code visualizes the refractive-index contrast Δn normalized to the smallest refractive-index contrast Δn_0: $\alpha = \Delta n / \Delta n_0$ (in the illustrated design $\Delta n_0 \equiv \Delta n_{\mathrm{WG1}}$). The curvatures of WG1 and WG3 are identical, and so are the minimum separation distances s_0 between the lateral waveguides and WG2. The z position of s_0 is different: WG2 and WG3 are initially closer than WG1 and WG2 [$C_P(0) \ll C_S(0)$ and $C_P(L) \gg C_S(L)$, with L being the length of the device]. Injection in WG1 (at $z = 0$) corresponds to a counterintuitive order of the coupling constants and injection in WG3 to in an intuitive order. This shape of waveguides is kept unchanged throughout this work. The only variable parameters are the three relative refractive-index contrasts α_1, α_2, and α_3 used to choose the mode conversion and the regime (STIRAP or AE). In the following BPM simulations, $L = 30$ mm, $\Delta n_0 = 0.004$, $s_0 = 9.6$ μm, and the width of the waveguides is $w = 8$ μm.

the beam-propagation method (BPM). The example calculations show that both STIRAP and AE systems lead to a robust mode conversion from a high-order mode to the fundamental one or from a fundamental to high-order mode over a broad spectral range.

II. THEORETICAL BACKGROUND

We consider a system of three evanescently coupled dielectric waveguides, such as the one shown in Fig. 1, where each waveguide $i = 1$, 2, or 3 can have a different refractive-index contrast Δn_i. Δn_i is represented by the normalized refractive-index contrast $\alpha_i = \Delta n_i / \Delta n_0$, where Δn_0 is the smallest refractive-index contrast, corresponding to that of WG1 in Fig. 1. The main goal of this work is to achieve a mode converter in which one mode is injected into an input waveguide, WGI (WG1 or WG3), and is converted to another mode at the exit of the device in the opposite lateral waveguide, WGO (WG3 or WG1). Therefore, adjusting α_i selects the propagation constants β of the excited mode in each waveguide. Even though we treat explicitly a variation of β by a variation of the whole contrast in planar-type waveguides, the theory exposed in this section is general. The propagation constants can be adjusted by tuning any of the waveguide parameters, for instance, the lateral core dimensions instead of the index contrast.

The wave propagation can be analyzed in the framework of coupled-wave theory [51]. We consider multimode waveguides with no perturbation. The excited mode in each waveguide depends on the design parameters of the waveguides and on the injected light. We can assume that,

with a proper injection, only one mode propagates in each waveguide. For an efficient mode converter the propagation constants β_{I_j} of mode j injected in WGI and β_{O_k} of mode k in WGO must be matched: $\beta_{I_j} = \beta_{O_k} = \bar{\beta}$. In the following, we do not limit our analysis to configurations where the central WG2 is also phase matched, so $\beta_{2_m} = \bar{\beta} + \Delta\beta$, where m refers to mode m excited in WG2 through coupling of the adjacent waveguides. Like the other waveguides, WG2 can be multimode; therefore, the mode excited in WG2 corresponds to the one associated with the smallest $\Delta\beta$ [52,53]. The assumption of the propagation of a single mode in each waveguide is justified for the designs considered in the next section, where only a few modes are supported by the waveguides with well-separated propagation constants. Under such conditions, the propagation of the electric-field amplitudes $a_1(z)$, $a_2(z)$, and $a_3(z)$ of the waves traveling in the three waveguides is described by the following system of three coupled differential equations written in matrix form:

$$i\frac{d}{dz}\begin{bmatrix} a_1 \\ a_2 \\ a_3 \end{bmatrix} = \begin{bmatrix} 0 & C_{12}e^{-i\Delta\beta z} & 0 \\ C_{21}e^{i\Delta\beta z} & 0 & C_{23}e^{i\Delta\beta z} \\ 0 & C_{32}e^{-i\Delta\beta z} & 0 \end{bmatrix}\begin{bmatrix} a_1 \\ a_2 \\ a_3 \end{bmatrix}, \quad (1)$$

where $C_{lr}(z)$ are the z-dependent coupling coefficients from waveguide r to waveguide l and, in general, $C_{lr} \neq C_{rl}$ since C_{lr} (C_{rl}) is associated with mode-distribution overlap in waveguide l (r) [53,54]. The longitudinal z variation of the coupling constants is associated with the changing distance between the waveguides seen in Fig. 1. The direct coupling between WG1 and WG3 is neglected because the structure is assumed to be planar and their separation distance is supposed to be sufficiently large.

Similar to the approach given in [55], Eq. (1) can be set in a more symmetric form using $a_1' = \sqrt{C_{21}/C_{12}}\, a_1$, $a_2' = \exp(-i\Delta\beta z)\, a_2$, and $a_3' = \sqrt{C_{23}/C_{32}}\, a_3$:

$$i\frac{d}{dz}\begin{bmatrix} a_1' \\ a_2' \\ a_3' \end{bmatrix} = \begin{bmatrix} 0 & C_P & 0 \\ C_P & \Delta\beta & C_S \\ 0 & C_S & 0 \end{bmatrix}\begin{bmatrix} a_1' \\ a_2' \\ a_3' \end{bmatrix}, \quad (2)$$

where the pump (C_P) and the Stokes (C_S) coupling constants are geometrical averages of the above coefficients C_{lr}, i.e., $C_P \equiv \sqrt{C_{12}C_{21}}$ and $C_S \equiv \sqrt{C_{23}C_{32}}$, named similarly to the parameters for quantum STIRAP [56,57]. To ensure an adiabatic transfer, the z dependence of $C_P(z)$ and $C_S(z)$ must remain moderate, meaning a smooth enough z dependence of the waveguide parameters, a long enough waveguide length, and a large enough coupling [41].

When there is no propagation constant mismatch ($\Delta\beta = 0$), with counterintuitive sequences of the coupling constants, the light propagation in the coupled waveguides is analogous to the three-state STIRAP. A counterintuitive configuration means that C_S is stronger than C_P in the first half of the propagation for injection in WG1, as in Fig. 1. This should lead to a robust transfer from WG1 to WG3, with only a little transient light in WG2 [35,36,39]. To conceive a mode converter and not only an adiabatic coupler, the only additional constraint is to match the propagation constants of WG1 and WG3 for different modes. The mode conversion could concern any two modes, for instance, converting a high-order mode to the fundamental one or vice versa. Note that, contrary to earlier work

on STIRAP in coupled waveguides, the condition $\Delta\beta = 0$ can correspond to various designs of WG2. WG2 can be identical to WGI or WGO or can even be different from the other two as long as at least one mode is matched to the propagation constant $\bar{\beta}$.

In a standard directional coupler composed of two coupled waveguides, the case $\Delta\beta \neq 0$ is associated with incomplete power transfer. However, in an adiabatic three-waveguide coupler an efficient and complete conversion may occur even in the presence of mismatch. Moreover, it was shown in quantum physics that even strong detuning can lead to efficient and robust population transfer. This effect is called adiabatic elimination since it virtually eliminates the intermediate state [46,50]. It was exploited and demonstrated experimentally in coupled waveguides for broadband couplers [55,58]. Indeed, when

$$\frac{|\Delta\beta|}{\sqrt{C_P^2 + C_S^2}} \gg 1, \tag{3}$$

the derivative of $a_2'(z)$ varies rapidly, and the average values of $a_2'(z)$ and $a_2(z)$ over many cycles will be zero; thus, the average of the derivative vanishes as well: $da_2'(z)/dz = 0$. If no light is initially input in the middle waveguide, this extreme limit leads to a strong suppression of the wave amplitude in WG2 throughout the propagation, like for STIRAP. Equation (2) can then be reduced to an effective two-state system, lacking the middle waveguide [55],

$$i\frac{d}{dz}\begin{bmatrix} \tilde{a}_1 \\ \tilde{a}_3 \end{bmatrix} = \begin{bmatrix} -\Delta_{\text{eff}} & C_{\text{eff}} \\ C_{\text{eff}} & \Delta_{\text{eff}} \end{bmatrix}\begin{bmatrix} \tilde{a}_1 \\ \tilde{a}_3 \end{bmatrix}, \tag{4}$$

where $a_i'(z)$ is replaced by $\tilde{a}_i'(z)$ after the addition of an unimportant phase shift ($\tilde{a}_i(z) \equiv \exp[-i(C_P^2 + C_S^2)z/(2\Delta\beta)]a_i'(z)$). The quantity

$$\Delta_{\text{eff}} \equiv \frac{C_P^2 - C_S^2}{2\Delta\beta} \tag{5}$$

in Eq. (4) is an effective detuning, and

$$C_{\text{eff}} \equiv -\frac{C_P C_S}{\Delta\beta} \tag{6}$$

is an effective coupling coefficient. Therefore, in the adiabatic regime, the light intensity contained in WG1 and WG3 varies, and adiabatic evolution can produce energy transfer between the outer waveguides with no light in WG2. For the case of the structure shown in Fig. 1 and the examples that will be discussed in Secs. III and IV, when light enters WG1 and goes out WG3, the effective phase mismatch Δ_{eff} sweeps from some negative to some positive value. This is exactly the mechanism that is at work also in the rapid-adiabatic-passage-like two-waveguide system with explicit detuning of the propagation constants [59]. In multimode waveguides, the value of Eq. (3) is limited since the switching occurs only with the modes associated with minimal $\Delta\beta$. Moreover, adiabatic propagation requires a strong coupling C_{eff}. In this kind of system, there is always a sort of compromise to find suitable conditions. More details on the theory of AE for waveguides can be found in Ref. [55]. Note that the switch in the sign of Δ_{eff} along z can be in one direction or the other, which has the consequence that both the intuitive and CI orders of coupling

will lead to complete light transfer from WGI to WGO, that is, in both situations (WGI $\equiv$ WG1 or WGI $\equiv$ WG3) in the configuration in Fig. 1. This is not the case for STIRAP, where WGI must be WG1. As already mentioned, these adiabatic transfers can be adapted quite easily to realize simultaneously a mode conversion as long as the propagation constant of the injected mode j in WGI β_{I_j} is identical to the propagation constant of the output mode k in WGO $\beta_{O_k} = \beta_{I_j} = \bar{\beta}$, with $j \neq k$. This will be verified in Sec. III by means of BPM simulations for the two configurations of STIRAP ($\Delta\beta = 0$) and AE [$\Delta\beta$ verifies Eq. (3)]. We will also discuss what happens in intermediate situations where neither $\Delta\beta = 0$ nor Eq. (3) is fulfilled. Note that this theory is rather general and can be applied to any type of dielectric waveguide, independently of the geometry or technology involved.

III. EXAMPLES OF MODE CONVERTERS BASED ON STIRAP AND AE

In this section, we choose, as an example, to verify the above expectations by performing numerical simulations of the wave propagation in the planar structures in Fig. 1. A BPM algorithm using a split-step Fourier method is used for the simulations [60,61]. To take a realistic example, the waveguides are assumed to be written in fused silica, for which the cladding refractive index is 1.4440 at 1550 nm [62]. For the sake of simplicity we consider that all waveguides are planar waveguides with an identical width $w = 8$ µm and WG1 and WG3 have the same parabolic curvature, represented in Fig. 1, to ensure proper evolution of $C_P(z)$ and $C_S(z)$. The minimum separation distance $s_0 = 9.6$ µm (the distance between the centers of two adjacent waveguides). The total propagation length is $L = 30$ mm to get a slow adiabatic evolution.

We first design a mode converter based on STIRAP transfer ($\Delta\beta = 0$). The starting situation corresponds to normalized refractive-index profiles in each waveguide: $\alpha_1 = \alpha_2 = \alpha_3 = 1$ in Fig 1, equivalent to a refractive-index contrast $\Delta n = 0.004$ in all waveguides. In that case, all waveguides are matched, and the fundamental mode (mode 0) is launched in WGI $\equiv$ WG1 at $z = 0$ (ensuring a CI configuration). We use the nomenclature ST_000 to reference this first case since it is based on STIRAP (ST_) and the mode 0 is excited in all three waveguides (000). Such a systematic naming is used throughout this work for greater clarity and easier comparison of the different cases. The corresponding designations and parameters are given in Table I.

As expected and as shown in Fig. 2(a), for ST_000 the BPM propagation shows a direct light transfer from WG1 to WG3 with no transient light in WG2 and no oscillation from one waveguide to the other. This provides evidence that the design is suitable for adiabatic transfer. Therefore, the system can be very easily tuned to build a mode converter based on STIRAP by adjusting the output propagation constant until $\beta_{O_k} = \beta_{I_0}$, with $k \neq 0$, is reached. Standard mode resolution in a rectangular-slab waveguide gives $\beta_{I_0} = \bar{\beta} = 5.86$ µm^{-1} at the wavelength $\lambda = 1550$ mn for $\alpha_I = 1$ [53]. With $\alpha_O \equiv \alpha_3 = 2.4$ we obtain $\beta_{O_1} = \bar{\beta}$ for the first-order mode (mode 1) and $\beta_{O_2} = \bar{\beta}$ with $\alpha_O = 5.3$ for the second-order mode (mode 2). These two situations are simulated respectively in Fig. 2(b) (ST_001) and Fig. 2(c) (ST_002), where α_2 is kept fixed to 1.

TABLE I. Nomenclature of the various simulated cases, used for easier reference, with the corresponding relative refractive-index contrasts α_I, α_2, and α_O and matched propagation constants at the wavelength $\lambda = 1.55$ μm. In the nomenclature "Name_I2O," "Name" designates a propagation analog to STIRAP (ST) or AE, and the three numbers "I2O" denote the propagating modes in WGI, WG2, and WGO.

Name_I2O	α_I	α_2	α_O	Matching conditions at 1.55 μm
ST_000	1	1	1	$\beta_{I_0} = \beta_{2_0} = \beta_{O_0}$
ST_001	1	1	2.4	$\beta_{I_0} = \beta_{2_0} = \beta_{O_1}$
ST_002	1	1	5.3	$\beta_{I_0} = \beta_{2_0} = \beta_{O_2}$
ST_011	1	2.4	2.4	$\beta_{I_0} = \beta_{2_1} = \beta_{O_1}$
AE_021	1	5.6	2.4	$\beta_{I_0} = \beta_{O_1} < \beta_{2_2}$
AE_021b	1	7	2.4	$\beta_{I_0} = \beta_{O_1} \ll \beta_{2_2}$
AE_022	1	5.6	5.3	$\beta_{I_0} = \beta_{O_2} < \beta_{2_2}$
AE_120	2.4	5.6	1	$\beta_{I_1} = \beta_{O_0} < \beta_{2_2}$

It can clearly be seen that perfect mode conversions occur along with adiabatic light transfer: mode 0 injected in WG1 is converted to mode 1 or 2 at the output of WG3. Of course, the design can also be used to convert a higher-order mode to the fundamental one by injecting the high-order mode in WG3
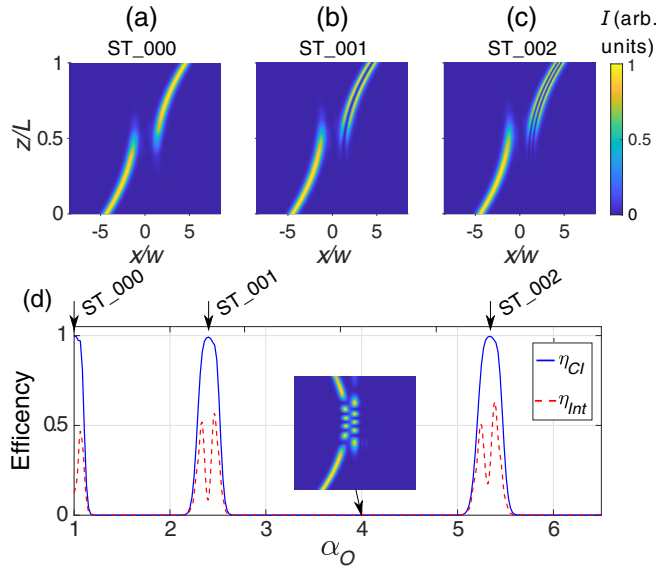

FIG. 2. (a)–(c) show the propagation of light obtained by BPM simulations at the wavelength $\lambda = 1.55$ μm, where the shape of the waveguides corresponds to Fig. 1 with $\alpha_I \equiv \alpha_1 = 1$ (CI case, with injection of mode 0) and $\alpha_2 = 1$. $\alpha_O \equiv \alpha_3$ is changed to match three different modes: (a) $\alpha_O = 1$, case ST_000 in Table I, (b) $\alpha_O = 2.40$, case ST_001, and (c) $\alpha_O = 5.33$, case ST_002. The color code visualizes the normalized light intensity going from 0 (blue) to 1 (yellow). This illustrates three different cases of STIRAP-like transfer with mode conversion for (b) and (c). (d) Evolution of the transfer efficiencies [Eq. (7)] with the parameter α_O ($\alpha_I = \alpha_2 = 1$). The blue solid curve shows the counterintuitive case (η_{CI}), and the red dashed curve gives the intuitive case (η_{Int}). The three maxima where $\eta_{CI} = 1$ correspond to propagations (a), (b), and (c). The small inset illustrates the beam propagation for $\alpha_O = 4$, where all modes of the output waveguide are mismatched.

at $z = L$ (or by injection in WG1 at $z = 0$ with a permutation of α_1 and α_3).

Even without calculating the propagation modes, this first two cases of mode conversion, ST_001 and ST_002, can be found again in Fig. 2(d), where we consider a variation of the output waveguide index contrast (variation of α_O). Specifically, Fig. 2(d), shows the α_O dependence of the transfer efficiency

$$\eta = \frac{P_O(z = L)}{P_I(z = 0)}, \qquad (7)$$

where $P_O(z = L)$ is the output power in WGO and $P_I(z = 0)$ is the initial power launched in WGI. The two curves represent η_{CI} for the counterintuitive case (WGI $\equiv$ WG1 and WGO $\equiv$ WG3) and η_{Int} for the intuitive case (WGI $\equiv$ WG3 and WGO $\equiv$ WG1).

Several remarks can be made. First, $\eta_{CI} = 1$ is obtained at the expected values of α_O, but the range where $\eta_{CI} > 0.5$ is quite large, which gives the first indication of a robust behavior. Note also that when $\eta < 1$, light is distributed in several output ports, but a pure output mode is always observed. This means there is no mode mixing since the choice of the excited mode in WG2 and WGO is forced due to evanescent coupling. Another remark is that, with the intuitive configuration, η_{Int} never reaches 1 and strongly oscillates around mode matching. This two points will be analyzed in more detail in the following. Finally, except around the mode-matching condition, there is never any light in WGO. Indeed, since $\alpha_I = \alpha_2$, there is a strong coupling from WGI to WG2, and the light oscillates between these two waveguides (similar to Rabi oscillations in quantum dynamics). This is like in any resonant coupler, and no transfer occurs to unmatched WGO. The inset in Fig. 2(d) illustrates this behavior for the CI case with $\alpha_O = 4$.

As detailed in Sec. II, adiabatic mode conversion should also occur when $\Delta\beta \neq 0$, especially when the AE condition is fulfilled [Eq. (3)]. To get the whole picture, we plot in Fig. 3 the evolution of η_{CI} and η_{Int} as a function of α_O and α_2 while keeping $\alpha_1 = 1$. The white dashed lines correspond to the profiles in Fig. 2(d). We focus on the beginning of the dynamics for $\alpha_O < 6.5$ and $\alpha_2 < 20$, but the dynamics repeats for higher values. This gives further evidence that α_O must correspond to $\beta_{O_k} \approx \beta_{I_0}$ to get high efficiency, as already shown in Fig. 2(d). Indeed, the three vertical regions with $\eta \approx 1$ correspond to the first three mode-matching conditions, between WGI and WG3, obtained for $\alpha_O = 1$ ($\beta_{I_0} = \beta_{O_0}$), $\alpha_O = 2.4$ ($\beta_{I_0} = \beta_{O_1}$), and $\alpha_O = 5.3$ ($\beta_{I_0} = \beta_{O_2}$), which were already discussed. Around these conditions, η is close to 1 for almost all values of α_2 for the CI propagation and also for the intuitive case. Indeed, an essential condition for quantum STIRAP is the two-photon resonance [63], which is analogous here to $\beta_{I_0} = \beta_{O_k}$, as already mentioned in Sec. II. On the contrary, when α_2 varies [i.e., $\Delta\beta$ in Eq. (2) varies], the analogy to single-photon resonance in quantum STIRAP is lost. This additional resonance condition is less critical since the intermediate state is never populated. This explains the large range of α_2 values associated with $\eta \approx 1$. Moreover, both counterintuitive [Fig. 3(a)] and intuitive [Fig. 3(b)] cases are extremely similar except precisely around the conditions corresponding to a perfect STIRAP ($\beta_{I_0} = \beta_{2_m} = \beta_{O_k}$), where η_{Int}
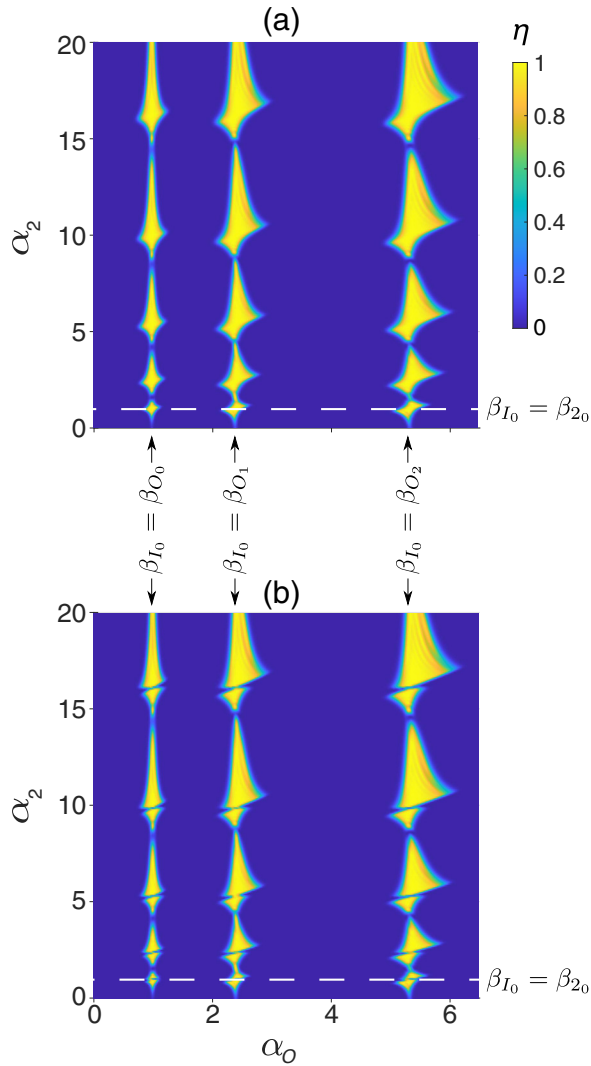
FIG. 3. (a) Color plot of η_{CI} as a function of α_O and α_2 for the counterintuitive case at $\lambda = 1.55$ μm. (b) Corresponding η_{Int} for the intuitive case. All the others waveguide parameters are as in Fig. 1 ($\alpha_I = 1$). At the positions of the white dashed lines ($\alpha_2 = 1$), the efficiencies correspond to the profiles in Fig. 2(d). The three vertical regions with $\eta \approx 1$ correspond to $\beta_{I_0} \approx \beta_{O_k}$ for the first three modes.
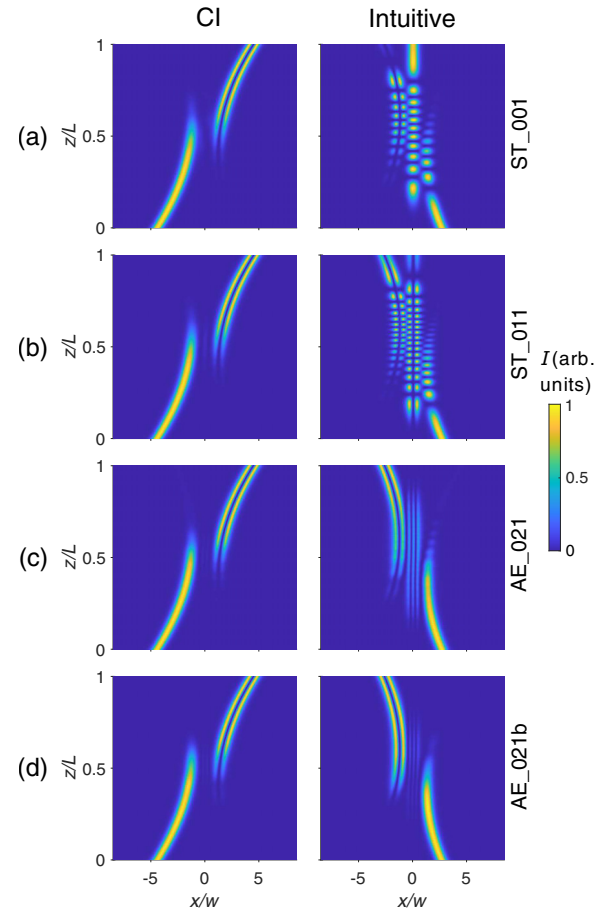

FIG. 4. Examples of beam conversions from mode 0 ($\alpha_I = 1$) to mode 1 ($\alpha_O = 2.4$) illustrated by the evolution of light intensities at $\lambda = 1.55$ μm in the waveguide design in Fig. 1, except for α_2, which varies: (a) $\alpha_2 = 1$, ST_001 [the CI case corresponds to Fig. 2(b)], (b) $\alpha_2 = 2.4$, ST_011, (c) $\alpha_2 = 5.6$, AE_021, and (d) $\alpha_2 = 7$, AE_021b. The left column shows the CI cases, and the right one shows the intuitive ones. (a) and (b) show two converters based on STIRAP, while (c) and (d) illustrate AE configurations where both CI and intuitive propagations lead to robust mode conversion. In (d) the AE condition of Eq. (3) is better verified, and therefore, almost no light transits to WG2, even in the intuitive case. The color code shows the normalized light intensity.

falls. This shows that even a moderate verification of the AE condition of Eq. (3) is sufficient for efficient mode conversion in the intuitive order of the coupling constants. However, the presence of WG2 is essential, as seen for $\alpha_2 \to 0$, where $\eta \to 0$. This also proves that there is no direct coupling from WG1 to WG3. Figure 3(a) also shows that in each yellow region, corresponding to $\eta_{\text{Int}}(\alpha_O) \approx 1$ and shaped like a "spinning top," the maximum horizontal extensions of strong efficiencies are obtained around the condition $\beta_{I_0} = \beta_{2_m}$, giving the first indication of how a STIRAP configuration is more robust than an AE one.

For a better understanding of these results, we show in Fig. 4 the beam propagation for several interesting cases for the CI (left column) and intuitive (right column) cases for a mode conversion from mode 0 to mode 1 where only α_2 is modified. All CI cases show efficient adiabatic mode conversions. ST_001 and ST_011, in Figs. 4(a) and 4(b), correspond to the first STIRAP transfers for the CI cases with $\beta_{I_0} = \beta_{2_0} = \beta_{O_1}$ in Fig. 4(a) and $\beta_{I_0} = \beta_{2_1} = \beta_{O_1}$ in Fig. 4(b). For the intuitive order of the coupling constants (right panels), it is clearly seen that, in these resonant cases, the "population" of the intermediate state (WG2) strongly oscillates. Therefore, depending on the values of the coupling constants, a significant part of the light can exit through WG2 or WG3 with no robust transfer, as expected by theory. For AE_021 and AE_021b [Figs. 4(c) and 4(d)], the matched-propagation-constant condition $\beta_{I_0} = \beta_{O_1}$ is still verified; therefore, the CI propagations are the same as the STIRAP ones. On the contrary, for the intuitive propagations, each case leads to an efficient transfer to mode 1 in WGO, as already suggested in Fig. 3(b). The difference between Figs. 4(c) and 4(d) is the transient light in WG2, which is much more important
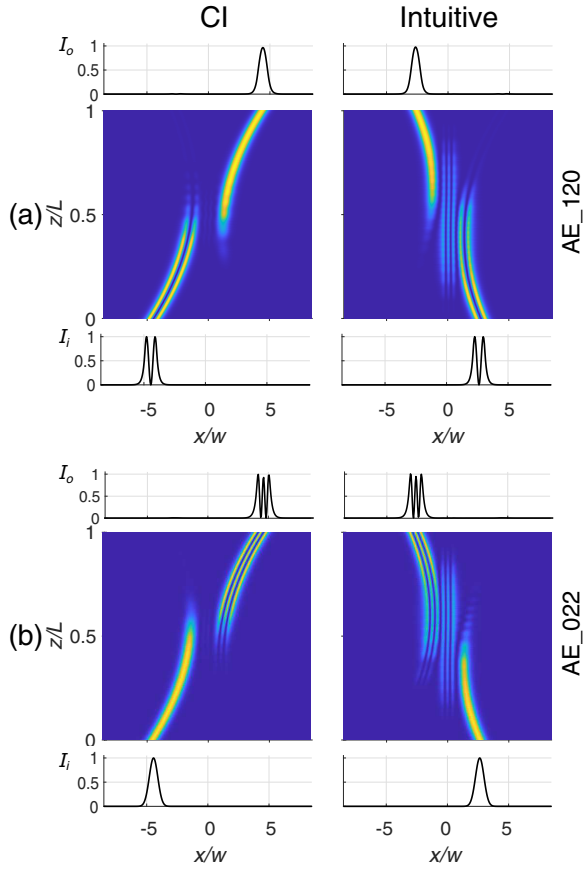
FIG. 5. Examples of other possible conversions illustrated by the evolution of light intensities at $\lambda = 1.55$ μm in the waveguide designs in Fig. 1, except for α_I and α_O ($\alpha_2 = 5.6$ as in Fig. 1). (a) $\alpha_I = 2.4$ and $\alpha_O = 1$ (AE_120), realizing conversion from mode 1 to 0, and (b) $\alpha_I = 1$ and $\alpha_O = 5.33$ (AE_022), realizing conversion from mode 0 to 2. The left column shows the CI case, and the right one shows the intuitive case. The color code shows the normalized light intensity. The top profiles (bottom profiles) show the output (input) transverse intensity profiles.

in Fig. 4(c) than in Fig. 4(d). Indeed, the AE criterion of Eq. (3) is >5 for AE_021b [Fig. 4(d)] instead of ≈ 1 for AE_021 [Fig. 4(c)], justifying the better elimination of WG2 for the case in Fig. 4(d). Nevertheless, even for the intuitive propagation of AE_021, the dynamic is quite different from the intuitive resonant cases since there is no light oscillation: the light coupled to WG2 conserves a rather constant intensity before escaping to WGO. One could also note that for the designs AE_021 and AE_021b, the excited mode in WG2 is mode 2 since it corresponds to the mode with the smallest mismatch $\Delta\beta$.

Additional examples of adiabatic mode conversions are given in Fig. 5, where we add the injected light intensity profiles (bottom panels) and the output ones (top panels). For AE_120 [Fig. 5(a)] mode 1 is injected in the waveguide with the higher refractive index. This shows that our concept can be used not only for mode conversion from the fundamental to a higher-order mode but also for conversion to the fundamental one. The light profiles give further visual evidence of the strong efficiencies. The last example, AE_022, in Fig. 5(b),

illustrates mode conversion from mode 0 to mode 2, with the same WG2 ($\alpha_2 = 5.6$) as for AE_021 [Fig. 4(c)]. Another case of conversion to mode 2 based on STIRAP has already been shown with ST_002 [Fig. 2(c)]. Other cases for mode conversion from mode 0 to 2 are not shown, but the dynamics are the same as for conversion from mode 0 to 1. Moreover, our concept can be extended to any mode conversion. These examples clearly demonstrate the strong potential of this mode-conversion technique, where no mode mixing can occur as long as the parameters of the waveguides are kept constant along the propagation distance. Robust transfers are also obtained since the efficiency does not need precise phase-matching conditions. This robust behavior should also lead to a broadband operation, which is studied in the next section.

IV. SPECTRAL ANALYSIS

The variation of mode-conversion efficiency η with wavelength λ is plotted in Fig. 6 for the various cases discussed in the previous section. The refractive-index contrasts Δn are supposed to be fixed (independent of λ), but the dispersion of fused silica is taken into account for the cladding refractive index. Figures 6(a) and 6(b) correspond to designs ST_001 and ST_011, which show broadband efficiencies only for the CI cases (blue solid curves), as expected for STIRAP transfers. Due to the different spectral evolution of the propagation constants in waveguides with different Δn, the overall phase matching $\beta_{O_k} = \beta_{I_0}$ is lost by tuning λ. This phase mismatch between waveguides WGI and WGO with λ is the main parameter limiting the bandwidth of the mode converters. Moreover, for ST_001 [Fig. 6(a)], $\beta_{I_0}(\lambda) = \beta_{2_0}(\lambda)$ is verified at all wavelengths, whereas for ST_011 [Fig. 6(b)], it is the condition $\beta_{O_1}(\lambda) = \beta_{2_1}(\lambda)$ which is fulfilled. Matching WG2 with the highest lateral mode results in an increased bandwidth. Matching the central waveguide with the highest refractive-index contrast is always preferential since the maximum coupling constant increases with the mode order, which leads to better fulfillment of adiabatic evolution. Therefore, for the chosen parameters, a bandwidth >250 nm can be reached for our 01 mode converter. In the intuitive cases in Figs. 6(a) and 6(b), strong variations of η_{Int} (red dashed curves) occur around phase matching at $\bar{\lambda} = 1.55$ μm, as expected from STIRAP theory, and no efficient robust transfer occurs.

In the AE situations in Figs. 6(c)–6(e), the λ-dependent phase mismatch between WGI and WGO is again the main driving parameter limiting the bandwidth. However, since WG2 is phase matched with neither WGI nor WGO, the bandwidth is therefore smaller than for CI propagation using STIRAP. Case AE_021 in Fig. 6(c) is an intermediate AE situation where the initial detuning with WG2 at $\bar{\lambda} = 1.55$ μm is moderate and reaches almost zero around $\lambda = 1.63$ μm, explaining the big dip in η_{Int} at this wavelength. For longer λ, the detuning increases rapidly, like in the other situations, and the efficiency drops in a way similar to what occurs in the other cases. Therefore, the interest of AE mode conversion in comparison with STIRAP is not the bandwidth, but the very similar broadband behavior for the CI and intuitive cases. This is of practical importance since the same device could be used for signals propagating forward or backward: mode 0
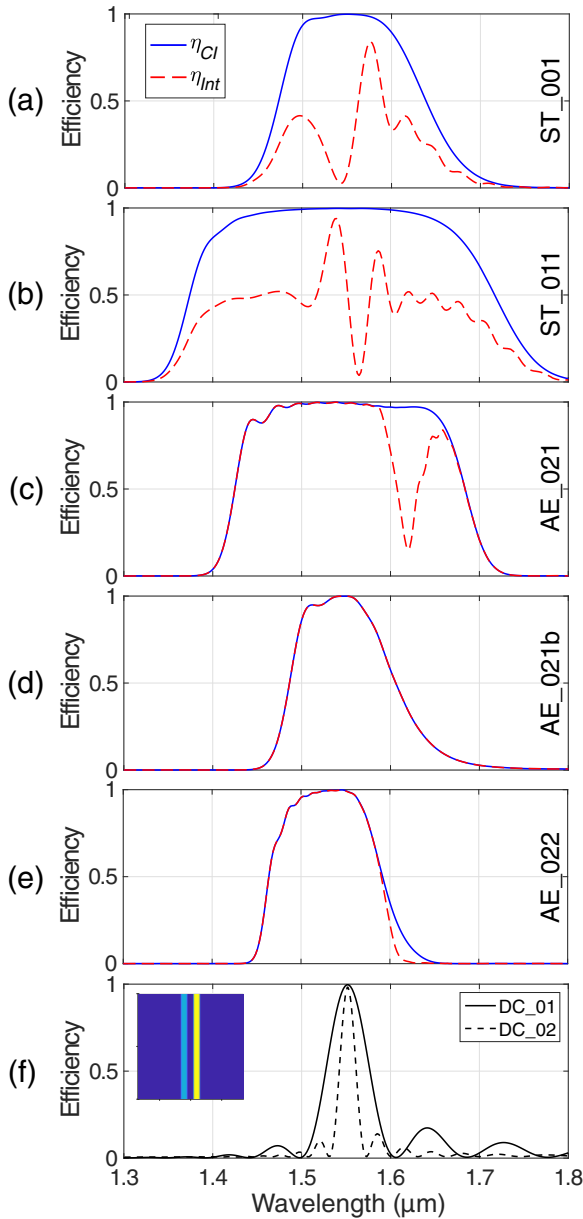
FIG. 6. Evolution of η_{CI} (solid blue curve) and η_{Int} (dashed red curve) as a function of wavelength λ. (a)–(d) are for conversion from mode 0 ($\alpha_I = 1$) to mode 1 ($\alpha_O = 2.4$). (e) is for conversion from mode 0 to mode 2 ($\alpha_O = 5.33$). The panels differ by the refractive-index contrasts in WG2: (a) $\alpha_2 = 1$ [ST_001, with the corresponding beam propagation at $\bar{\lambda} = 1.55$ μm in Fig. 4(a)], (b) $\alpha_2 = 2.4$ [ST_011, corresponding to Fig. 4(b)], (c) $\alpha_2 = 5.6$ [AE_021, corresponding to Fig. 4(c)], (d) $\alpha_2 = 7$ [AE_021b, corresponding to Fig. 4(d)], and (e) $\alpha_2 = 5.6$ with $\alpha_O = 5.33$ [AE_022, corresponding to Fig. 5(b)]. (f) shows conversions based on standard directional couplers for comparison. The solid curve is for conversion from mode 0 to mode 1 ($\alpha_O = 2.4$, DC_01), and the dashed curve is for conversion to mode 2 ($\alpha_O = 5.33$, DC_02). The design of the two straight waveguides is shown in the inset with $L = 6.5$ mm and $s_0 = 2w$ for all z; the others parameters are the same as before.

can enter WG1 in both directions (at $z_I = 0$ or at $z_I = L$) and is converted to mode 1 in WG3 at the exit (at $z_O = L$ or at $z_O = 0$), while mode 1 can enter WG3 in both directions and

is converted to mode 0 in WG1 at the exit. Therefore, unlike for the STIRAP-like designs, four input and output ports can be used.

The curves for AE_022 in Fig. 6(e) show the bandwidth of the 02 mode converter where the propagation at $\bar{\lambda} = 1.55$ is in Fig. 5(b). This example shows that going to a higher-order mode does not affect the bandwidth much, especially for AE configurations. Nevertheless, the bandwidth tends to decrease by going to higher-order modes. Indeed, the higher the mode is, the faster the propagation constant changes with λ. This AE_022 example is of particular interest since it uses the same WG2 ($\alpha_2 = 5.6$) as AE_021, demonstrating that the same intermediate waveguide can be used for different mode conversions. For the 02 conversion in Fig. 6(e), the dip seen in Fig. 6(c) is no longer present. The reason is that the matching with WG2 is no longer in the wavelength range of strong efficiencies. AE conversions lead to smaller bandwidths than the CI STIRAP cases; nevertheless, all adiabatic mode converters are always much more broadband than a standard directional mode coupler, where the spectrum efficiencies for the 01 and 02 mode converters are plotted in Fig. 6(f). These directional coupler examples also illustrate the expected smaller bandwidth when going to higher-order modes. Note that the results in Fig. 6 are obviously the same when considering the conversion from a higher-order mode to the fundamental one.

V. CONCLUSIONS AND DISCUSSION

We proposed a rather simple method to realize broadband mode converters based on a system of three evanescently coupled waveguides, where all the parameters of the waveguides, such as the width and the refractive-index contrasts, remain constant for the entire propagation distance. The only changing parameter is the separation distance between the waveguides, giving an adiabatic evolution of the coupling constants in analogy with Hamiltonian interactions in quantum systems, such as STIRAP and adiabatic elimination. We demonstrated that these two approaches can be a fruitful inspiration to build broadband mode converters. Implementations in optics of STIRAP and AE for mode conversions are very similar, and we showed that changing only the refractive-index contrast of the intermediate waveguide is sufficient to select one process or the other.

Practical implementation of a different refractive-index contrast would require, for instance, a different doping concentration of the impurities or changing the doping element from one waveguide to another one. Alternatively, mode matching in different spatial modes can also be obtained for a common index contrast for all waveguides, but with different waveguide widths. This could be especially useful in the case of ridge waveguides. With this second design, which is not shown here in the simulations but is formally identical, the refractive-index contrasts are usually stronger; therefore, strong coupling requires smaller separation distances, which could reduce the footprint of the devices.

Finally, we have shown that AE has the advantage of permitting strong tolerance in the parameter of the central

waveguide and gives components with four useful input and output ports. However, the STIRAP-like waveguide structure exhibits a larger bandwidth that can reach 250 nm at telecommunication wavelengths in the given examples, again without requiring any complex longitudinal variation of the waveguides. The same devices can be used for mode conversion from a low-order mode to a higher-order mode or vice versa. This concept can be extended to others functionalities, such as mode multiplexing or demultiplexing. The broadband behavior would permit us to combine such adiabatic mode converters with wavelength multiplexing easily.

[1] D. J. Richardson, J. M. Fini, and L. E. Nelson, Nat. Photonics **7**, 354 (2013).

[2] S. G. Leon-Saval, N. K. Fontaine, J. R. Salazar-Gil, B. Ercan, R. Ryf, and J. Bland-Hawthorn, Opt. Express **22**, 1036 (2014).

[3] J. Wang, Y. Xuan, M. Qi, H. Huang, Y. Li, M. Li, X. Chen, Z. Sheng, A. Wu, W. Li, X. Wang, S. Zou, and F. Gan, Opt. Lett. **40**, 1956 (2015).

[4] S.-Y. Tseng and M.-C. Wu, IEEE Photon. Technol. Lett. **22**, 1211 (2010).

[5] M.-C. Wu, F.-C. Hsiao, and S.-Y. Tseng, IEEE Photonics Technol. Lett. **23**, 807 (2011).

[6] H. Qiu, H. Yu, T. Hu, G. Jiang, H. Shao, P. Yu, J. Yang, and X. Jiang, Opt. Express **21**, 17904 (2013).

[7] R. Xiao, Y. Shi, J. Li, P. Dai, Y. Zhao, L. Li, J. Lu, and X. Chen, Opt. Express **27**, 1941 (2019).

[8] M. Minz and R. K. Sonkar, Appl. Opt. **60**, 2640 (2021).

[9] K. Nakamura, T. Fujisawa, T. Sakamoto, T. Matsui, K. Nakajima, and K. Saitoh, J. Opt. Soc. Am. B **38**, 946 (2021).

[10] H. Xu and Y. Shi, Opt. Lett. **41**, 5047 (2016).

[11] H. Li, P. Wang, T. Yang, T. Dai, G. Wang, S. Li, W. Chen, and J. Yang, Opt. Laser Technol. **100**, 7 (2018).

[12] F. Callewaert, S. Butun, Z. Li, and K. Aydin, Sci. Rep. **6**, 32577 (2016).

[13] C. Zhu, Y. Xu, Z. Kang, X. Hu, Y. Dong, B. Zhang, Y. Ni, and P. Xu, Photonics **8**, 95 (2021).

[14] Z. Guo, S. Wu, and J. Xiao, J. Lightwave Technol. **39**, 5563 (2021).

[15] W. Jiang and S. Xu, J. Lightwave Technol. **39**, 6239 (2021).

[16] M. Heinrich, M.-A. Miri, S. Stützer, R. El-Ganainy, S. Nolte, A. Szameit, and D. N. Christodoulides, Nat. Commun. **5**, 3698 (2014).

[17] S. Longhi, Opt. Lett. **40**, 463 (2015).

[18] C. P. Tsekrekos and D. Syvridis, IEEE Photonics Technol. Lett. **24**, 1638 (2012).

[19] T. Uematsu, Y. Ishizaka, Y. Kawaguchi, K. Saitoh, and M. Koshiba, J. Lightwave Technol. **30**, 2421 (2012).

[20] D. González-Andrade, J. G. Wangüemert-Pérez, A. V. Velasco, A. Ortega-Moñux, A. Herrero-Bermello, I. Molina-Fernández, R. Halir, and P. Cheben, IEEE Photonics J. **10**, 1 (2018).

[21] Y. Xu, C. Zhu, X. Hu, Y. Dong, B. Zhang, and Y. Ni, J. Opt. Soc. Am. B **37**, 1290 (2020).

[22] Z. Guo, S. Wu, and J. Xiao, J. Lightwave Technol. **40**, 2060 (2022).

[23] L.-W. Luo, N. Ophir, C. P. Chen, L. H. Gabrielli, C. B. Poitras, K. Bergmen, and M. Lipson, Nat. Commun. **5**, 3069 (2014).

[24] B. Stern, X. Zhu, C. P. Chen, L. D. Tzuang, J. Cardenas, K. Bergman, and M. Lipson, Optica **2**, 530 (2015).

[25] V. Liu, D. A. B. Miller, and S. Fan, Opt. Express **20**, 28388 (2012).

[26] O. M. Nawwar, H. M. H. Shalaby, and R. K. Pokharel, Opt. Lett. **43**, 4176 (2018).

[27] D. Ohana and U. Levy, Opt. Express **22**, 27617 (2014).

[28] Z. Li, M.-H. Kim, C. Wang, Z. Han, S. Shrestha, A. C. Overvig, M. Lu, A. Stein, A. M. Agarwal, and M. Lončar, Nat. Nanotechnol. **12**, 675 (2017).

[29] H. Wang, Y. Zhang, Y. He, Q. Zhu, L. Sun, and Y. Su, Adv. Opt. Mater. **7**, 1801191 (2019).

[30] L. Hao, Y. Zhao, Y. Wu, Z. He, Y. Shi, R. Xiao, P. Dai, T. Fang, Z. Han, and X. Chen, IEEE Photonics Technol. Lett. **32**, 1143 (2020).

[31] F.-C. Hsiao, T.-Y. Lin, and S.-Y. Tseng, IEEE Photonics J. **3**, 1198 (2011).

[32] W. Jiang, S. Xu, and H. Zhang, IEEE Photonics Technol. Lett. **33**, 415 (2021).

[33] Z. L. Hussain and R. S. Fyath, Optik **264**, 169456 (2022).

[34] S. Longhi, Laser Photonics Rev. **3**, 243 (2009).

[35] N. V. Vitanov, A. A. Rangelov, B. W. Shore, and K. Bergmann, Rev. Mod. Phys. **89**, 015006 (2017).

[36] E. Paspalakis, Opt. Commun. **258**, 30 (2006).

[37] B. M. Rodríguez-Lara, H. M. Moya-Cessa, and D. N. Christodoulides, Phys. Rev. A **89**, 013802 (2014).

[38] H. S. Hristova, A. A. Rangelov, G. Montemezzani, and N. V. Vitanov, Phys. Rev. A **93**, 033802 (2016).

[39] S. Longhi, G. Della Valle, M. Ornigotti, and P. Laporta, Phys. Rev. B **76**, 201101(R) (2007).

[40] F. Dreisow, A. Szameit, M. Heinrich, S. Nolte, A. Tunnermann, M. Ornigotti, and S. Longhi, Phys. Rev. A **79**, 055802 (2009).

[41] C. Ciret, V. Coda, A. A. Rangelov, D. N. Neshev, and G. Montemezzani, Phys. Rev. A **87**, 013806 (2013).

[42] S.-Y. Tseng and M.-C. Wu, J. Lightwave Technol. **28**, 3529 (2010).

[43] W. Song, S. Wu, Y. Chen, C. Chen, S. Gao, C. Huang, K. Qiu, S. Zhu, and T. Li, Phys. Rev. Appl. **17**, 014039 (2022).

[44] G. Della Valle, Phys. Rev. A **98**, 053861 (2018).

[45] H. Liu and L.-F. Wei, IEEE J. Quantum Electron. **57**, 1 (2021).

[46] L. A. Lugiato, P. Mandel, and L. M. Narducci, Phys. Rev. A **29**, 1438 (1984).

[47] A. Sinatra, F. Castelli, L. Lugiato, P. Grangier, and J. Poizat, Quantum Semiclassical Opt. **7**, 405 (1995).

[48] M. Fewell, Opt. Commun. **253**, 125 (2005).

[49] E. Brion, L. H. Pedersen, and K. Mølmer, J. Phys. A **40**, 1033 (2007).

[50] B. W. Shore, Acta Phys. Slovaca **58**, 243 (2008).

[51] A. Yariv, IEEE J. Quantum Electron. **9**, 919 (1973).

[52] R. Olshansky, Appl. Opt. **14**, 935 (1975).

[53] D. Marcuse, *Theory of Dielectric Optical Waveguides*, 2nd ed. (Academic Press, London, 1991).

[54] E. Marcatili, IEEE J. Quantum Electron. **22**, 988 (1986).

[55] H. Oukraou, V. Coda, A. A. Rangelov, and G. Montemezzani, Phys. Rev. A **97**, 023811 (2018).

[56] U. Gaubatz, P. Rudecki, S. Schiemann, and K. Bergmann, J. Chem. Phys. **92**, 5363 (1990).

[57] N. V. Vitanov, T. Halfmann, B. W. Shore, and K. Bergmann, Annu. Rev. Phys. Chem. **52**, 763 (2001).

[58] M. Mrejen, H. Suchowski, T. Hatakeyama, Y. Wang, and X. Zhang, Nano Lett. **15**, 7383 (2015).

[59] H. Oukraou, L. Vittadello, V. Coda, C. Ciret, M. Alonzo, A. A. Rangelov, N. V. Vitanov, and G. Montemezzani, Phys. Rev. A **95**, 023811 (2017).

[60] J. V. Roey, J. van der Donk, and P. E. Lagasse, J. Opt. Soc. Am. **71**, 803 (1981).

[61] K. Kawano and T. Kitoh, *Introduction to Optical Waveguide Analysis: Solving Maxwell's Equations and the Schrödinger Equation* (Wiley, New York, 2001).

[62] I. H. Malitson, J. Opt. Soc. Am. **55**, 1205 (1965).

[63] N. V. Vitanov, M. Fleischhauer, B. W. Shore, and K. Bergmann, Adv. At., Mol., Opt. Phys. **46**, 55 (2001).